The Astrophysical Journal, 572:55–65, 2002 June 10

A MEASUREMENT OF WEAK LENSING BY LARGE-SCALE STRUCTURE IN RED-SEQUENCE CLUSTER SURVEY FIELDS

Henk Hoekstra,[1,2,3] Howard K. C. Yee,[2,3,4] Michael D. Gladders,[2,3,4] L. Felipe Barrientos,[4,5] Patrick B. Hall,[2,3,4,5,6] and Leopoldo Infante[4,5]

Received 2001 September 26; accepted 2002 February 14

ABSTRACT

We have analyzed $\sim$24 deg^2 of R_C-band imaging data from the Red-Sequence Cluster Survey (RCS) and measured the excess correlations between galaxy ellipticities on scales ranging from 1′ to 30′. We have used data from two different telescopes: $\sim$16.4 deg^2 of Canada-France-Hawaii Telescope data and $\sim$7.6 deg^2 of Cerro Tololo Inter-American Observatory 4 m data, distributed over 13 widely separated patches. For the first time, a direct comparison can be made of the lensing signal measured using different instruments, which provides an important test of the weak-lensing analysis itself. The measurements obtained from the two telescopes agree well. For the lensing analysis, we use galaxies down to a limiting magnitude of $R_C = 24$, for which the redshift distribution is known relatively well. This allows us to constrain some cosmological parameters. For the currently favored ΛCDM model ($\Omega_m = 0.3$, $\Omega_\Lambda = 0.7$, $\Gamma = 0.21$), we obtain $\sigma_8 = 0.81^{+0.14}_{-0.19}$ (95% confidence), in agreement with the 2001 results from Van Waerbeke and coworkers, who used fainter galaxies (and consequently higher redshift galaxies). The good agreement between these two very different weak-lensing studies demonstrates that weak lensing is a useful tool in observational cosmology.

Subject headings: cosmology: observations — dark matter — gravitational lensing

1. INTRODUCTION

Weak gravitational lensing has proven to be a powerful tool for studies of the mass distribution in rich clusters of galaxies (for a review, see Mellier 1999). Since the pioneering work by Tyson, Wenk, & Valdes (1990), much progress has been made, and in the present day, the weak-lensing signals induced by clusters of galaxies at intermediate redshifts can be measured without much difficulty.

The development of advanced techniques to correct for the various observational distortions, such as the anisotropy of the point-spread function (PSF), the circularization by the PSF, and the camera-induced distortion, has been a crucial step, resulting in well-calibrated signals (e.g., Kaiser, Squires, & Broadhurst 1995; Luppino & Kaiser 1997; Hoekstra et al. 1998; Kuijken 1999; Refregier 2001). Another important development in recent years is the advent of mosaic CCD cameras, which enable us to quickly image large portions of the sky.

These advances have made it possible to pursue one of the most difficult measurements in the field of weak lensing: the measurement of the coherent distortions of the images of faint galaxies caused by lensing by intervening large-scale structure, the so-called cosmic shear. The analysis of this lensing signal provides an important direct measurement of the statistical properties of the large-scale mass distribution (e.g., Blandford et al. 1991; Kaiser 1992; Bernardeau, Van Waerbeke, & Mellier 1997; Schneider et al. 1998).

Compared to many other methods that are used to constrain cosmological parameters, weak lensing has the advantage that no assumptions about the light distribution are required. However, weak lensing in itself cannot constrain all the parameters, because of degeneracies between them. Better constraints can be obtained by comparing weak-lensing studies that probe different redshifts (e.g., Hu 1999) or by combining these data with measurements of the fluctuations of the cosmic microwave background (e.g., Hu & Tegmark 1999).

By now, several groups have reported the detection of an excess correlation between galaxy ellipticities and have argued that this signal is caused by lensing by large-scale structure (e.g., Bacon, Refregier, & Ellis 2000; Kaiser, Wilson, & Luppino 2000; Van Waerbeke et al. 2000, 2001; Wittman et al. 2000; Maoli et al. 2001). Maoli et al. (2001) combined their own results with published measurements in an attempt to obtain constraints on σ_8, the normalization of the power spectrum, and Ω_m, the matter density of the universe. They found good agreement with studies of cluster abundances. However, the data set studied by Maoli et al. (2001) is very inhomogeneous, which limits the accuracy of such a direct comparison.

After these initial detections, which demonstrated the feasibility of the method, the obvious next step is to obtain large uniform data sets. The first results from such a survey were presented by Van Waerbeke et al. (2001), who measured a highly significant lensing signal from 6.5 deg^2 of deep imaging data.

In this paper we present the results from our analysis of $\sim$24 deg^2 of R_C-band data from the Red-Sequence Cluster Survey (RCS) (e.g., Gladders & Yee 2000), which is a 100 deg^2 galaxy cluster survey designed to provide a large sample of optically selected clusters of galaxies with redshifts

[1] Canadian Institute for Theoretical Astrophysics, University of Toronto, Toronto, ON M5S 3H8, Canada.

[2] Department of Astronomy and Astrophysics, 60 Saint George Street, University of Toronto, Toronto, ON M5S 3H8, Canada.

[3] Visiting Astronomer, Canada-France-Hawaii Telescope, which is operated by the National Research Council of Canada, Le Centre National de Recherche Scientifique, and the University of Hawaii.

[4] Guest observer at the Cerro Tololo Inter-American Observatory (CTIO), a division of the National Optical Astronomy Observatory, which is operated by the Association of Universities for Research in Astronomy, Inc., under cooperative agreement with the National Science Foundation.

[5] Departamento de Astronomía y Astrofísica, Avenida Vicuña Mackenna 4860, Universidad Católica de Chile, Casilla 306, Santiago 22, Chile.

[6] Princeton University Observatory, Princeton, NJ 98544-1001.

$0.1 < z < 1.4$. The data are also useful for a range of lensing studies. For example, Gladders, Yee, & Ellingson (2002) presented the first results for one of the strong lensing clusters discovered in the survey, for which follow-up observations are underway.

The weak-lensing applications are numerous. The survey imaging data are relatively shallow compared to what is common in weak-lensing studies, and as a result, the statistical uncertainty in the measurements of individual structures (such as clusters of galaxies) is large. However, thanks to the large survey area, many such structures can be detected, and by stacking the signals, one can study their ensemble-averaged mass distribution (e.g., Hoekstra et al. 2001b). In addition, follow-up observations will provide detailed information on individual systems.

In this paper we concentrate on the measurement of the weak-lensing signal induced by large-scale structure (cosmic shear). A study of galaxy biasing, based on some of these data, is presented in Hoekstra, Yee, & Gladders (2001a), and a study of the properties of galaxy halos is currently underway.

Compared to other cosmic shear studies, the RCS data are shallow, and consequently the signal at a given scale is much lower, as is the signal-to-noise ratio. However, measuring the weak-lensing signal from a shallow survey also has several advantages. Down to a limiting magnitude of $R_C \sim 24$, star-galaxy separation works well. In deeper surveys, many sources have sizes comparable to the size of the PSF, and applying size cuts may change the redshift distribution of the sources in a systematic way. In addition, down to $R_C \sim 24$, the redshift distribution of the sources is fairly well determined. In order to relate the observed cosmic-shear signal to cosmological parameters, a good understanding of the source redshift distribution is crucial.

One worry is the effect of intrinsic alignments of the source galaxies, which introduces an additional signal (e.g., Heavens, Refregier, & Heymans 2000; Catelan, Kamionkowski, & Blandford 2001; Crittenden et al. 2001; Mackey, White, & Kamionkowski 2002). The amplitude of the effect is not well determined, but it is clear that it becomes more important for shallower surveys. However, the predictions indicate that for a median redshift of $z = 0.5$ (which is similar to our sample of source galaxies), the signal caused by intrinsic alignments is still small compared to the lensing signal (e.g., Mackey et al. 2002), and we ignore the effect in this paper.

In § 2 we describe the RCS, from which we have used the R_C-band data for the analysis presented here. Section 3 deals with the analysis of the data, as well as the corrections for systematic distortions, such as PSF anisotropy and the distortion by the camera. In § 4 we discuss the expected signal from weak lensing by large-scale structure. The results of the analysis are presented in § 5.

2. DATA

2.1. *The Red-Sequence Cluster Survey*

The RCS[7] is a galaxy cluster survey designed to provide a large sample of optically selected clusters of galaxies with redshifts $0.1 < z < 1.4$. The planned survey covers 100 deg^2 in both R_C and z', and consists of 22 widely separated patches of $\sim 2^\circ.1 \times 2^\circ.3$. The northern half of the survey is observed using the CFH 12k camera on the Canada-France-Hawaii Telescope (CFHT), and the data from the southern half are obtained using the Mosaic II camera on the Cerro Tololo Inter-American Observatory (CTIO) 4 m telescope. The patches are imaged down to a 5 σ point source depth of 25.2 mag in the R_C band, and 23.6 mag in the z' filter.

For the weak-lensing analysis, we use only the R_C-band data, as these provide a sufficiently high number density of sources to warrant an accurate measurement of the lensing signal. We present the results based on $\sim$16.4 deg^2 of CFHT data and $\sim$7.6 deg^2 of CTIO data. In this paper we use a subset of the RCS, and the data for each patch are not contiguous. Thus, the largest scale we consider here is that of one pointing of the CFH 12k or Mosaic II camera.

We have used data from all 10 patches that have been observed using the CFHT, resulting in a total of 53 pointings. The integration times are 900 s per pointing. In addition, we have used three patches (resulting in an additional 23 pointings) from the first CTIO run, which have integration times of 1200 s. Some details about the observations are listed in Table 1.

2.2. *Data Reduction*

Given the large amount of data collected in the survey, special attention was paid during the survey design on how to handle the data flow. To simplify the construction of the science images, the data were acquired without dithering. Although the gaps between the chips, cosmetic defects, and cosmic rays result in a minor loss in area, the advantage in handling the data flow is tremendous. The loss of area does not affect the result of the weak-lensing analysis, and cosmic rays are easily removed from the galaxy catalogs.

The individual chips from the mosaic imagers are debiased and flat-fielded using standard techniques. The images are used for the object analysis, which is described below. A detailed discussion of the reduction pipeline is presented in M. D. Gladders & H. K. C. Yee (in preparation).

3. OBJECT ANALYSIS

Our weak lensing analysis technique is based on that developed by Kaiser et al. (1995) and Luppino & Kaiser (1997), with a number of modifications that are described in Hoekstra et al. (1998) and Hoekstra, Franx, & Kuijken (2000).

This correction scheme assumes that one can model the PSF as an isotropic function, convolved with a compact anisotropic kernel. The method does not make any assumptions about the profile of the PSF or the galaxy, as these parameters are measured from the actual data.

In real data, the PSF is likely to be more complex, and the assumption stated above is not valid. However, as shown by Hoekstra et al. (1998), matching the measurement of the PSF parameters to the size of the galaxy results in accurate corrections for PSFs with varying ellipticity as a function of radius (as is the case for the WFPC2 PSF).

In addition, the accuracy of this method has been studied in great detail (e.g., Erben et al. 2001; Bacon et al. 2001), and the results demonstrate that it works well down to the required accuracy for current data sets. Hence, the correc-

[7] See http://www.astro.utoronto.ca/~gladders/RCS.

TABLE 1
INFORMATION FOR THE POINTINGS USED IN THIS ANALYSIS

Patch	Pointing	Seeing (arcsec)	Run	Patch	Pointing	Seeing (arcsec)	Run
			CFHT				
0223	A2	0.72	2	1417	B2	0.61	1a
	A3	0.92	2		B3	0.61	1a
	A4	0.77	2		B4	0.52	1a
	A5	0.67	2		B5	0.59	1a
	B2	0.78	2	1447	A2	0.79	3
	B3	0.79	2		A3	0.74	3
	B4	0.64	2		B1	0.63	3
	B5	0.64	2		B2	0.66	2
0349	A1	0.69	2		B4	0.73	3
	A2	0.79	2	1614	A1	0.59	1a
	A3	0.87	2		A5	0.50	1a
	C1	0.63	2		B1	0.56	1a
	C2	0.59	2		B2	0.56	1a
0920	A2	0.73	2		B3	0.57	1a
	B1	0.70	2	2148	B2	0.63	1b
	B2	0.75	2		B3	0.65	1b
	C2	0.60	1a		B4	0.69	1b
	C3	0.69	1a		C1	0.89	1b
1120	A3	0.80	2		C2	0.82	1b
	A4	0.82	2	2316	A1	0.69	3
	B2	0.76	2		A2	0.66	3
	B3	0.67	2		A3	0.66	3
	B4	0.69	2		B3	0.72	3
1326	A3	0.74	2		B5	0.74	3
	A5	0.79	2				
	C1	0.58	1a				
	C2	0.55	1a				
	C3	0.58	1a				
			CTIO				
0333	A3	0.97	1	1102	A1	0.68	1
	A4	0.98	1		A2	0.75	1
	B3	0.88	1		A3	0.76	1
	B4	0.82	1		A4	0.82	1
	C3	1.03	1		B3	0.81	1
	C4	1.12	1		B4	0.77	1
0438	A1	0.80	1		C2	0.81	1
	A2	0.84	1		C3	0.86	1
	A3	0.87	1		C4	0.79	1
	A4	0.94	1				
	B3	0.89	1				
	B4	0.89	1				
	C3	0.94	1				
	C4	0.93	1				

NOTE.—With the CFHT, 10 widely separated patches were observed. Typically, five pointings per patch were used, except for the 1417 (four pointings) and 0223 (eight pointings) patches. With the CTIO, we used all the data obtained during run 1, and as a result, the number of pointings per patch varies. The seeing was determined for both telescopes using the sizes of stars on chip 3.

tion scheme is accurate even if the PSF does not satisfy the assumption made in the derivation. However, this can be understood easily, because any residuals induced by higher order moments of the PSF are suppressed as one averages the shapes of galaxies that have random orientations with respect to the PSF.

We analyzed the chips of each pointing separately. After the catalogs were corrected for the various observational effects, they were combined into a master catalog that covered the observed field (for each pointing).

The first step in the analysis was to detect the faint galaxy images, for which we used the hierarchical peak-finding algorithm from Kaiser et al. (1995). We selected objects that were detected with a significance greater than 5 σ over the local sky.

We used single exposures for our analysis, and consequently cosmic rays were not initially removed. However, cosmic rays were readily eliminated from the photometric catalogs: small but very significant objects are likely to be cosmic rays or artifacts from the CCD. The peak finder

gives fair estimates of the object size, and we removed all objects smaller than the size of the PSF.

The objects in this cleaned catalog were then analyzed, which yielded estimates for the size, apparent magnitude, and shape parameters (polarization and polarizabilities). The objects in this catalog were inspected by eye in order to remove spurious detections. These objects had to be removed because their shape measurements were affected by cosmetic defects (such as dead columns, bleeding stars, halos, and diffraction spikes) or because the objects were likely to be part of a resolved galaxy (e.g., H II regions). The visual inspection is important, as it is not possible to remove all spurious detections in a fully automatic process. Their removal is crucial for an accurate measurement of cosmic shear, because they increase the measurement of the variance and introduce artificial ellipticity correlations.

3.1. *Correction for the PSF*

To measure the small, lensing-induced distortions in the images of the faint galaxies, it is important to accurately correct the shapes for observational effects, such as PSF anisotropy and seeing; PSF anisotropy can mimic a cosmic-shear signal, and a correction for the seeing is required to relate the measured shapes to the real lensing signal.

To do so, we follow the procedure outlined in Hoekstra et al. (1998). We select a sample of moderately bright stars from our observations and use these to characterize the PSF anisotropy and seeing. Figure 1*a* shows a plot of the apparent R_C-band magnitudes of the detected objects versus their measured half-light radii for one of the chips of the A2 pointing of the 0223 patch (seeing $\sim 0\farcs77$). We have also indicated the region from which we have taken the stars used for the analysis of the PSF.

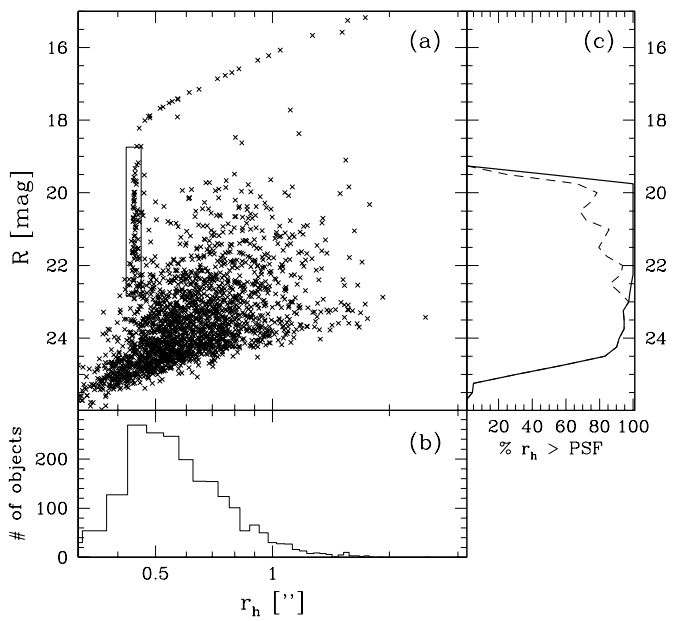

FIG. 1.—(*a*) Plot of the apparent R_C-band magnitude vs. the half-light radius. The vertical sequence of points at $r_h \sim 0\farcs45$ (indicated by the rectangle) consists of bright unsaturated stars that are used to study the PSF. (*b*) Histogram of the number of objects of given r_h. (*c*) Fraction of objects with half-light radii larger than the PSF (*dashed line*). The solid line shows the fraction of objects larger than the PSF when the total counts are corrected for the contribution by stars. Objects larger than the PSF are assumed to be galaxies, and only these are used in the weak-lensing analysis. The figure demonstrates that down to $R \sim 24$, this separation selects most galaxies, as almost all objects are larger than the PSF.

We fit a second-order polynomial to the shape parameters of the selected stars for each chip. This procedure is repeated for various dispersions of the weight function (for details, see Hoekstra et al. 1998). In Figure 2 (*left*) we present the resulting model PSF anisotropy for the A2 pointing of the 0223 patch. To show in more detail the higher order spatial dependence of the anisotropy, we have subtracted the average ellipticity. Although the fits were obtained from the individual chips, the mosaic image in Figure 2 shows continuity between the chips.

The results for one of the CTIO pointings is presented in Figure 2 (*right*). Comparison of the patterns presented in Figure 2 with other pointings shows that the pattern is fairly stable, although the amplitude varies because of focus variations. In general, the PSF anisotropy is small, a point that we address in more detail below, when we examine the residuals left after correction of the shapes of the galaxies used in the weak-lensing analysis.

3.2. *Telescope Distortion*

The effect of the PSF is not the only observational distortion that has to be corrected. The optics of the camera stretch the images of galaxies (i.e., they introduce a shear) because of the nonlinear remapping of the sky onto the CCD. We have used observations of astrometric fields to find the mapping between the sky and the CCD pixel coordinate system and have derived the corresponding camera shear.

The camera shear for the CFH 12k camera for run 2 is presented in Figure 3. The shear introduced by the camera is small, reaching a maximum value of $\sim 1\%$ at the edges of the field of view.

Other weak-lensing studies, which use dithered observations, need to remap the images before combining the data, thus removing the camera distortion. We have analyzed single exposures and measured the shapes of the galaxies on the reduced images that have not been remapped to remove the camera distortion. As discussed in Hoekstra et al. (1998), the images of both the stars and galaxies are sheared by the camera. The measured shape of the PSF (as shown in Fig. 2) is then the combination of PSF anisotropy and camera shear, and therefore the real PSF anisotropy is somewhat smaller than the measured value. The change in the ellipticity of an object caused by the camera shear depends on its shape (and hence the correction), whereas the PSF anisotropy correction depends mainly on the size of the object. As a result, the correction for PSF anisotropy leaves a residual ellipticity, because the correction is too large for larger galaxies. However, Hoekstra et al. (1998) demonstrated that the correction for the residual camera shear is straightforward: one just needs to subtract the camera shear from the measured shear, which is what we have done.

The camera shear is more or less radial with respect to the center of the camera (although the camera shear of the CTIO Mosaic II camera shows a significant nonradial component), which results in a negative tangential shear. It is therefore useful to examine the average tangential shear of the galaxies with respect to the center of the camera. The

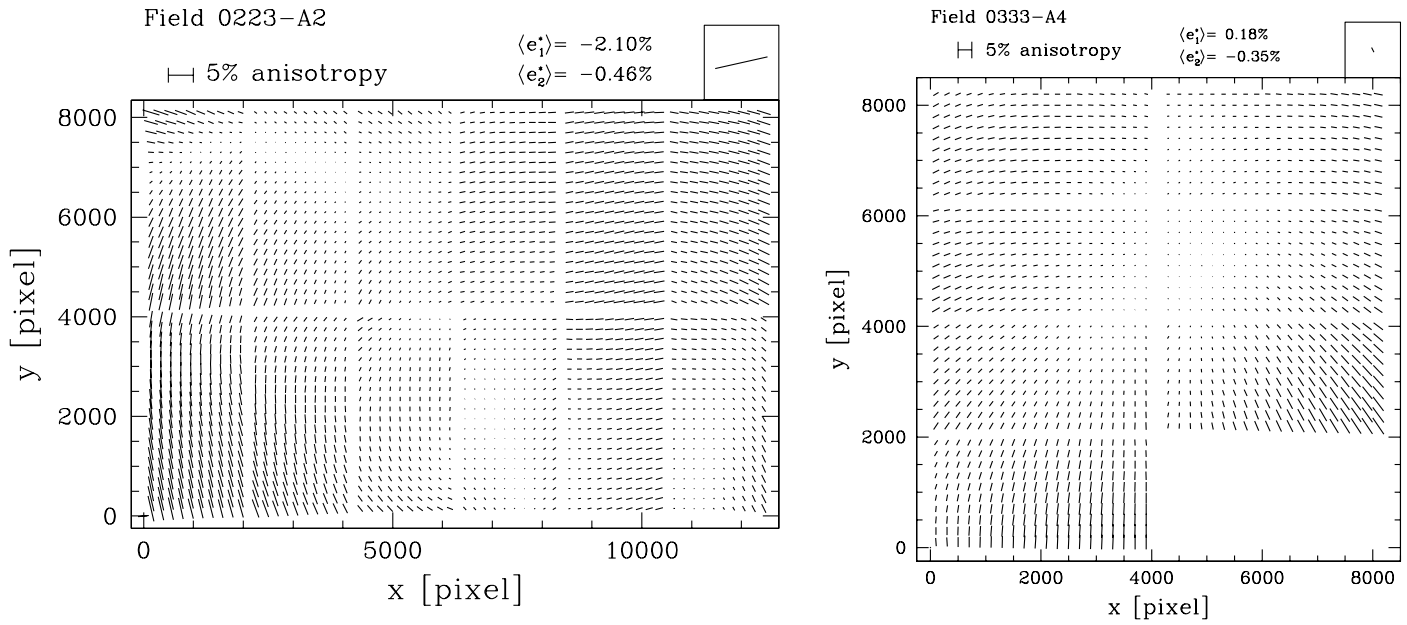

FIG. 2.—*Left*: PSF anisotropy as a function of position for one of the CFHT pointings. *Right*: PSF anisotropy for one of the CTIO pointings. One of the chips in the CTIO observations was not functioning and has been omitted. The sticks indicate the direction of the major axis of the PSF, and the length is proportional to the observed ellipticity of the PSF. In order to show the higher order spatial dependence of the anisotropy, we have subtracted the average ellipticity. The direction of the average PSF anisotropy is indicated in the top right box, and the amplitude is indicated as well. Although the PSF anisotropy was determined from fits to the observed shapes for individual chips, the figure clearly shows a large-scale dependence.

results are presented in Figure 4*a*. The filled circles indicate the average tangential distortion of the galaxies with respect to the center of the CFH 12k camera after correction for PSF anisotropy. These measurements agree well with the inferred camera shear (*solid line*). After subtracting the camera shear, we obtain the open circles, which are consistent with no signal.

3.3. *Residuals*

The correction scheme developed by Kaiser et al. (1995) has been tested extensively (e.g., Hoekstra et al. 1998; Bacon et al. 2001; Erben et al. 2001). The assumptions that have to be made to derive the original Kaiser et al. (1995) correction parameters do not necessarily hold in real data; the modifications suggested by Hoekstra et al. (1998) allow it to be applied to more complicated PSFs. This is supported by numerous simulations that indicate that the method works remarkably well down to the required accuracy for current data sets.

In addition, we have tested the method using a realistic simulation. The simulated data sets were created using the software tools SKYMAKER and STUFF,[8] which have been described in detail in Erben et al. (2001). The simulated galaxies have realistic profiles, with a mix of early-type and

[8] See http://terapix.iap.fr/soft.

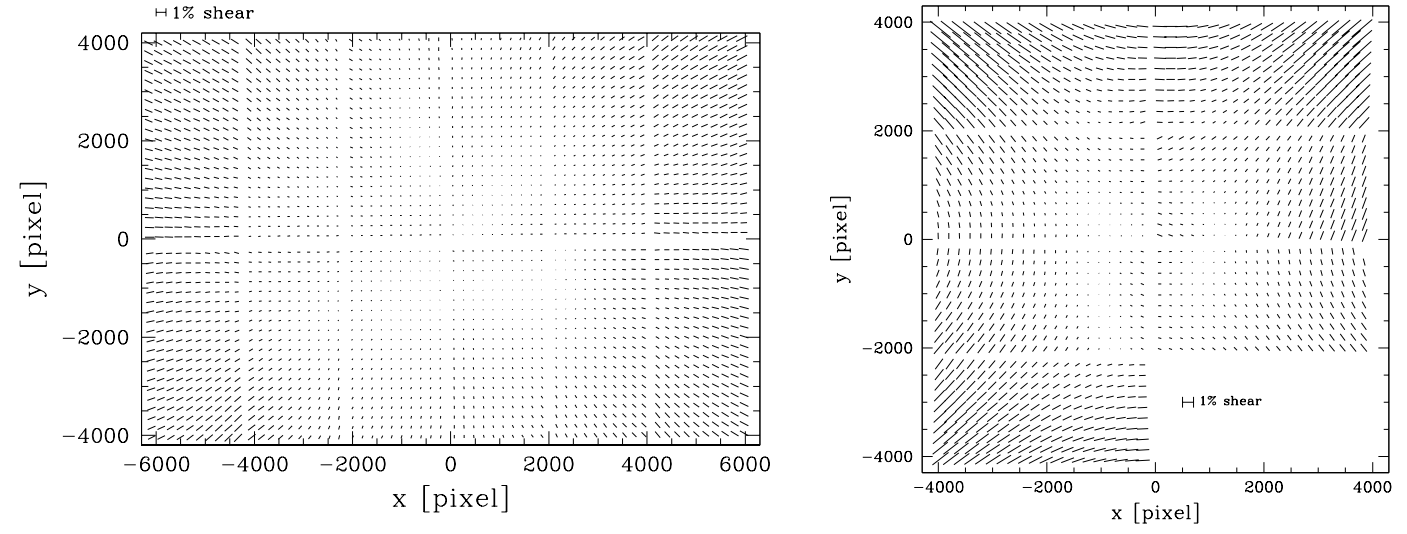

FIG. 3.—*Left*: Camera distortion measured for the CFH 12k camera for run 2. The shear introduced by the camera is small, reaching a maximum value of ~1% at the edges of the field of view. *Right*: Camera distortion measured from the CTIO data. One of the chips was not functioning and has been omitted. The induced shear by this camera is somewhat larger than the CFH 12k camera, but still small: ~2% at the edges of the field of view.

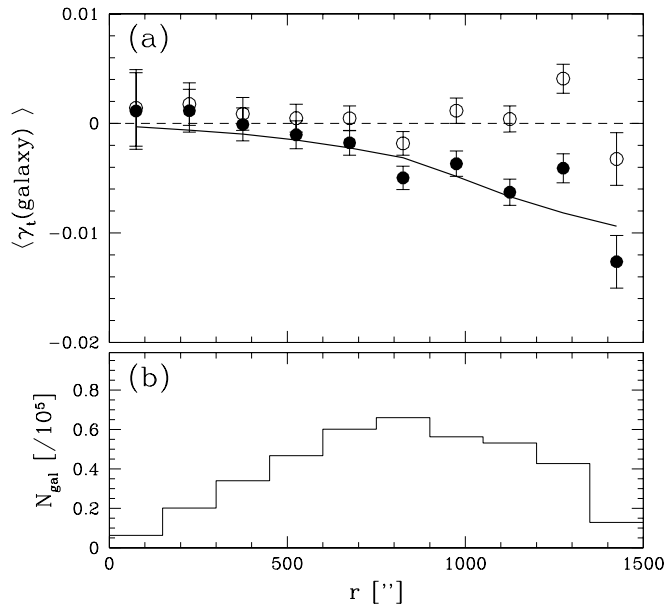

FIG. 4.—(*a*) Average tangential distortion of the galaxies with respect to the center of the CFH 12k camera after correction for PSF anisotropy (*filled circles*). The solid line corresponds to the average tangential camera shear. The open circles give the measurements of the galaxies after correcting for both PSF anisotropy and camera distortion. The results indicate that the two steps in the correction have worked well. (*b*) Number of galaxies as a function of radius used to produce (*a*).

late-type galaxies and disk/bulge ratios matched to actual observations. The PSF is computed using realistic pupil functions and includes all the problems encountered in real data, such as coma, tracking errors, aberration, spider arms from the support of the secondary mirror, etc.

The simulation is described by L. Van Waerbeke et al. (in preparation), and here we briefly discuss the results. Van Waerbeke used an *N*-body simulation to infer the corresponding (cosmic) shear by means of ray tracing. Artificial images of galaxies were sheared using these results. These galaxies were "observed," and the final images were convolved with a realistic PSF. A mosaic of 900 images (corresponding to $\sim$12 deg^2), each with a different PSF, was given to us. We note that the PSFs used in the simulation had worse systematics than the ones observed in the RCS data.

We analyzed these images in the same way as we have analyzed the RCS data and measured the cosmic shear signal. In doing so, we were able to recover the input lensing signal, which was unknown to us. We were able to recover the signal within 10% ($\sim$1 σ) of the input value. Because of the noise introduced by the intrinsic shapes of the galaxies, larger simulations are required to test whether we can measure the lensing signal to even higher accuracies.

We have also examined the residuals in the RCS data after PSF correction. A useful test, although not definitive, is to plot the average shape of the galaxies as a function of the shape of the PSF. The results for the two components of the shear are presented in Figure 5. Figures 5*c* and 5*f* indicate that the PSF anisotropy is small for most galaxies. The residuals presented in Figures 5*b* and 5*e* (note the different vertical scale) are consistent with no signal. The results of Figure 5 and the results from the simulation suggest that we are able to measure the lensing signal to an accuracy better than 10%.

4. COSMIC-SHEAR SIGNAL

To study the weak-lensing signal caused by large-scale structure, we use the top-hat smoothed variance of the shear (Bacon et al. 2000; Kaiser et al. 2000; Maoli et al. 2001; Van Waerbeke et al. 2000, 2001). Other statistics, such as the ellipticity correlation function (Kaiser 1992; Van Waerbeke et al. 2001; Wittman et al. 2000) or the aperture mass statistic (Schneider 1998; Schneider et al. 1998; Van Waerbeke et al. 2001) have also been used.

Here we briefly discuss how the lensing signal depends on the assumed cosmology and the redshift distribution of the sources. Detailed discussions on this subject can be found elsewhere (e.g., Schneider et al. 1998; Bartelmann & Schneider 2001).

Given a cosmological model, the variance in the shear caused by large-scale structure can be computed as a function of aperture size θ (e.g., Jain & Seljak 1997),

$$\langle\gamma^2\rangle(\theta) = 2\pi \int_0^\infty dl\, l P_\kappa(l) \left[\frac{J_1(l\theta)}{\pi l\theta}\right]^2 , \qquad (1)$$

where θ is the radius of the aperture used to compute the variance and J_1 is the first Bessel function of the first kind. The effective convergence power spectrum $P_\kappa(l)$ is given by

$$P_\kappa(l) = \frac{9H_0^4\Omega_m^2}{4c^4} \int_0^{w_h} dw \left[\frac{\bar{W}(w)}{a(w)}\right]^2 P_\delta\left(\frac{l}{f_K(w)};\ w\right) . \qquad (2)$$

Here w is the radial coordinate, w_h corresponds to the horizon, $a(w)$ is the cosmic scale factor, and $f_K(w)$ is the comoving angular diameter distance. As shown by Jain & Seljak (1997) and Schneider et al. (1998), it is necessary to use the nonlinear power spectrum in equation (2). This power spectrum is derived from the linear power spectrum following the prescriptions from Peacock & Dodds (1996).

The quantity $\bar{W}(w)$ is the source-averaged ratio of angular diameter distances D_{ls}/D_s for a redshift distribution of sources $p_w(w)$:

$$\bar{W}(w) = \int_w^{w_h} dw'\, p_w(w') \frac{f_K(w'-w)}{f_K(w')} . \qquad (3)$$

Thus, it is important to know the redshift distribution of the sources in order to relate the observed signal to $P_\kappa(l)$. A detailed discussion of the adopted redshift distribution can be found in § 4.1. Figure 6 shows the top-hat smoothed variance $\langle\gamma^2\rangle$ on a scale of 1′ as a function of limiting magnitude of the sample of sources. To compute the signal, we used galaxies with $20 < R < R_{\rm lim}$ and used the photometric redshift distribution inferred from the Hubble Deep Field–North and –South (see § 4.1). The top axis indicates the corresponding median redshift of the source galaxies.

One of the advantages of deep observations is obvious from Figure 6: the signal increases quickly for limiting magnitudes fainter than $R = 24$ (or higher median redshift). In addition, the number of sources increases as well, resulting in higher signal-to-noise ratios of the measurements.

4.1. *Redshift Distribution*

In order to relate the observed lensing signal to physical parameters, such as σ_8 or Ω_m, knowledge of the redshift distribution of the sources is crucial. The galaxies used in weak-lensing surveys are generally too faint to be included

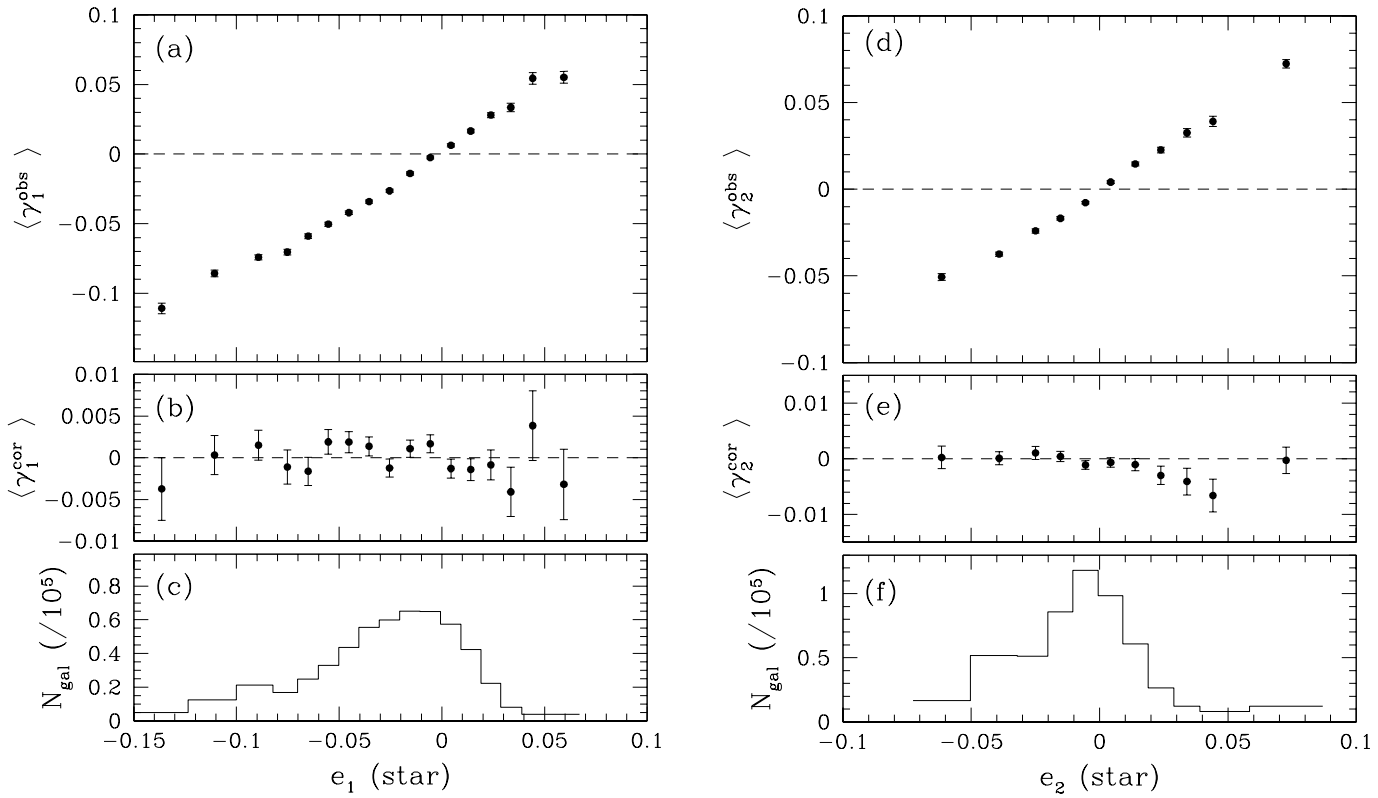

FIG. 5.—(a) Plot of $\langle\gamma_1\rangle$ for the galaxies with $20 < R < 24$ as a function of the value of the ellipticity component e_1 of the stars used to correct the galaxies. The results show the expected strong correlation. (*b*) Average γ_1 after correction for PSF anisotropy (note the vertical scale has been expanded with respect to [*a*]). (*c*) Number of galaxies with a given value for e_1 of the PSF. (*d*)–(*f*) Same as (*a*)–(*c*), but for γ_2. The residuals are consistent with no signal, demonstrating that the correction for the PSF anisotropy has worked well.

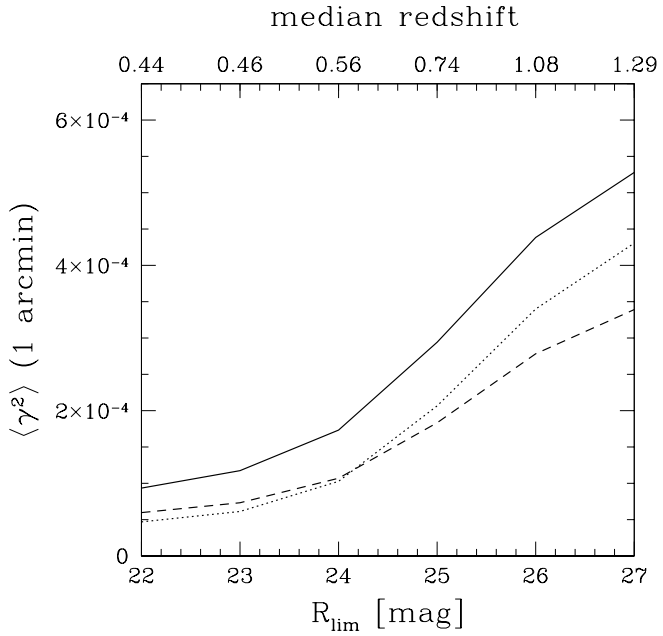

FIG. 6.—Expected variance induced by large-scale structure in an aperture of radius 1′, as a function of limiting magnitude of the source galaxies. To derive these results, we used source galaxies fainter than $R = 20$ and assumed perfect shape measurements. The results for the SCDM ($\Omega_m = 1$, $\Omega_\Lambda = 0$, $\sigma_8 = 0.5$, $\Gamma = 0.5$: *solid line*), OCDM ($\Omega_m = 0.3$, $\Omega_\Lambda = 0$, $\sigma_8 = 0.85$, $\Gamma = 0.21$: *dashed line*), and ΛCDM ($\Omega_m = 0.3$, $\Omega_\Lambda = 0.7$, $\sigma_8 = 0.9$, $\Gamma = 0.21$: *dotted line*) are shown. The cosmic shear signal increases rapidly with increasing limiting magnitude, or increasing median redshift (as indicated by the top axis).

in redshift surveys, and little is known about their redshift distribution from spectroscopic studies.

Compared to the other, deeper cosmic-shear studies, our analysis has the major advantage that the redshift distribution of the sources we use is better known. Down to a limiting magnitude of $R_C = 24$, the redshift distribution has been determined spectroscopically by Cohen et al. (2000), although this survey is limited to a relatively small patch of sky and is likely to suffer from cosmic variance.

In addition, the galaxies are larger, which is demonstrated in Figure 1: down to $R_C = 24$, the galaxies are easily separated from the stars. This has the advantage over deeper surveys (in which the fainter galaxies have sizes comparable to the PSF) in that selecting objects larger than the PSF does not change the redshift distribution significantly. Even for the worst seeing images considered here (∼1.″1), the stars are well separated from the galaxies for $R_C = 24$.

Photometric redshift studies, in particular those based on the Hubble Deep Fields (e.g., Fernández-Soto, Lanzetta, & Yahil 1999; Chen et al. 1998), have also provided important information. The results of Hoekstra et al. (2000) have demonstrated that they generally work well. However, Hoekstra et al. (2000) noted a difference between the redshift distributions inferred for the northern and the southern field, and such field-to-field variation is not unexpected. However, currently little is known about the amplitude of such variations, and more studies are required to constrain the redshift distributions of these faint galaxies.

In order to minimize the contribution of cosmic variance to the redshift distribution, we use the photometric redshift

distributions from Fernández-Soto et al. (1999) and Chen et al. (1998) to compute the predicted lensing signal for a given cosmology (see Fig. 2 from Hoekstra 2001 for the resulting redshift distribution). To do so, we have to take into account that the uncertainty in the shape measurements depends on the apparent magnitudes (and thus on the redshifts) of the sources: the contribution of distant, small, faint galaxies (with noisy shape measurements) to the measured lensing signal is smaller compared to that from brighter galaxies.

This is illustrated in Figure 7. Figure 7*a* shows the expected (based on modeling of deep number counts), the observed (galaxies for which shapes could be measured), and the effective number counts (*dotted line*) as a function of apparent magnitude. The effective number density takes into account the uncertainty in the galaxy shapes and gives a good indication of which galaxies contribute most to the measurement of the lensing signal. Based on the results displayed in Figure 7, we decided to use galaxies with $20 < R_C < 24$ for the lensing analysis.

The relative weight (normalized to unity for bright galaxies) as a function of magnitude is shown in Figure 7*b*. This weight function is simply the inverse square of the uncertainty in the shape measurement (see Hoekstra et al. 2000 for details) and reflects the fact that the shape estimates of faint galaxies are more noisy. We derive the "effective" redshift distribution using this weight function. This effective redshift distribution is used to compute the predicted lensing signals discussed in § 5.

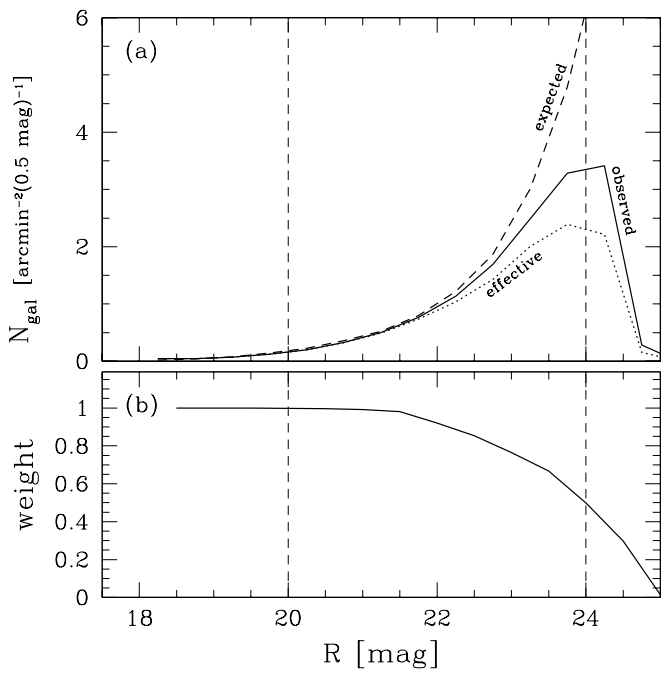

FIG. 7.—(*a*) Observed number density of galaxies (i.e., galaxies for which shapes could be determined) as a function of apparent R_C magnitude (*solid line*). The expected number density (based on modeling of observed number counts) is indicated by the dashed line. (*b*) Weight (based on the uncertainty in the shape measurements; see Hoekstra et al. 2000) multiplied by the completeness fraction as a function of apparent magnitude. The product of the number of galaxies and the weight gives a good indication of the relative contribution to the lensing signal (*dashed line in* [*a*].) The result shows that most of the signal comes from galaxies around $R_C = 23.5$. The vertical dashed lines indicate the region $20 < R_C < 24$, the range of apparent magnitudes for the source galaxies we use in the lensing analysis.

5. RESULTS

5.1. *Observed Signal*

In this section we present the measurement of the weak-lensing signal caused by large-scale structure using the top-hat smoothed variance of the shear. This statistic has been used by other groups to detect the cosmic-shear signal (e.g., Bacon et al. 2000; Kaiser et al. 2000; Maoli et al. 2001; Van Waerbeke et al. 2000, 2001). The top-hat smoothed variance is fairly insensitive to errors in the analysis because residual shears are added in quadrature. Consequently, the observed signal can always be considered as an upper limit, because residual errors always increase the variance. However, the results presented in Figure 5 and the simulations discussed in § 3.3 indicate that we can measure the shapes of the galaxies accurately.

As was found by Van Waerbeke et al. (2000), close pairs of galaxies can introduce an excess signal, because of overlapping isophotes. We therefore remove pairs with a separation of less than 2.″16 (which corresponds to 10 pixels for the CFHT data and 8 pixels for the CTIO data). This lowers the signal at small scales (∼20% for an aperture of radius 1′). We note that on these scales, intrinsic alignments can also be important. To compute the top-hat smoothed variance, we use the practical estimators given in Van Waerbeke et al. (2001).

Figure 8 shows the top-hat smoothed variance as a function of scale for both the CFHT data (*filled circles*) and the CTIO data (*open circles*) using galaxies with $20 < R_C < 24$. The error bars are estimated from a large number of random realizations of the data set in which the orientations of the galaxies were randomized.

Note that the measurements at various scales are strongly correlated, and this causes all the CTIO measurements at large scales to be higher than the CFHT results. The results obtained from the two different telescopes agree very well with one another. Because the systematics for the two data sets are different, this excellent agreement demonstrates that the various observational biases have been removed successfully.

Another useful test is to compare the signals from the individual patches. Figure 9 displays the top-hat smoothed variance of the shear for an aperture of radius 2.′5 (in which the signal-to-noise ratio is highest) for the 13 observed patches. The measurements for the individual patches agree with the ensemble average.

It is also important to examine the correction for the circularization by the PSF, because it determines the amplitude of the signal. To do so, we computed the variance on a scale of 2.′5 for each pointing and looked for a correlation with seeing. The results show no trend with seeing.

Figure 10 shows the measurement of the top-hat smoothed variance for the full weak-lensing data set . The signal-to-noise ratio of our measurements is very good, reaching a maximum of ∼6 at a radius of 2.′5.

For comparison, the predictions for three different cosmological models are also shown in this figure. All three models are good fits to the data, indicating the need for additional observational constraints (e.g., § 5.2).

It is difficult to compare our measurements directly with most other studies, because of the difference in the source redshift distribution (caused by the difference in filters and integration times). However, we can compare directly with the results from Bacon et al. (2000), who have used a similar

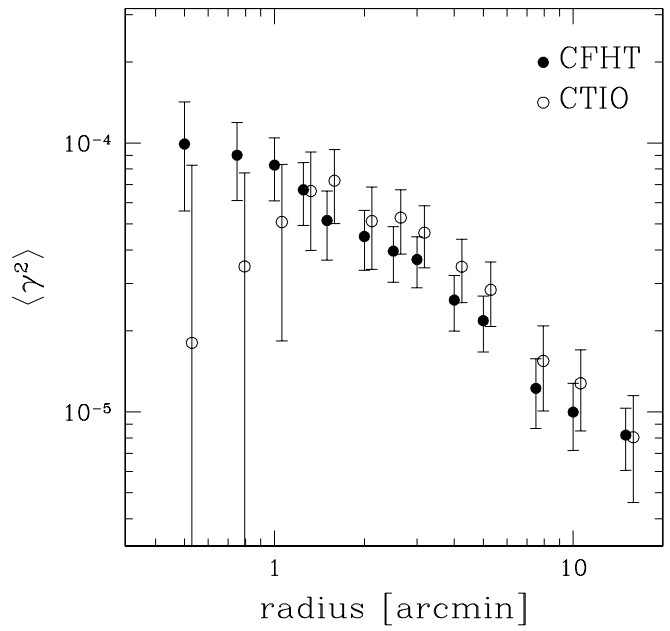

FIG. 8.—Top-hat smoothed variance of the shear as a function of aperture radius. The filled circles indicate the measurements based on 16.4 deg^2 of CFHT data, and the open circles correspond to the analysis of 7.6 deg^2 of CTIO data. For display purposes, the CTIO points have been offset slightly in radius. Note that the measurements at various scales are strongly correlated, and this causes all the CTIO measurements at large scale to be higher than the CFHT results. The results obtained from the two different telescopes agree well with one another.

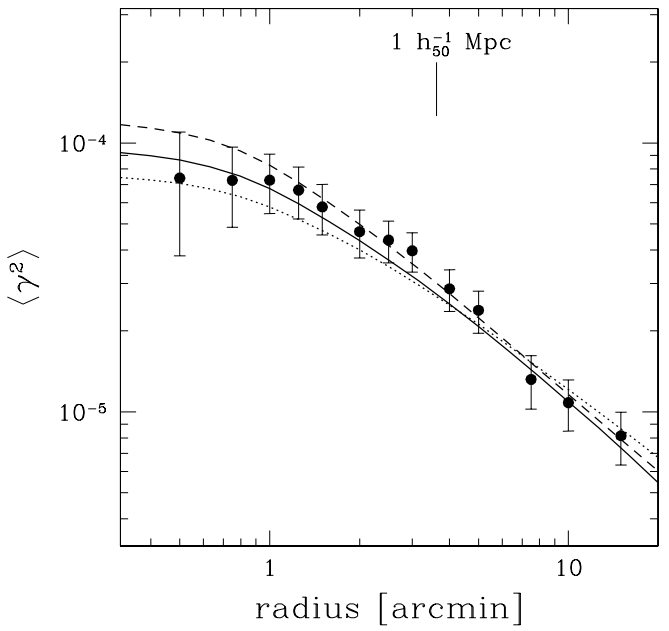

FIG. 10.—Measurement of the top-hat smoothed variance (excess variance caused by lensing by large-scale structure) using galaxies with $20 < R_C < 24$. The data consist of 16.4 deg^2 of CFHT data and 7.6 deg^2 of CTIO data. The drawn lines correspond to the best-fit SCDM ($\Omega_m = 1$, $\Omega_\Lambda = 0$, $\Gamma = 0.7$, $\sigma_8 = 0.31$: *solid line*), the best-fit OCDM ($\Omega_m = 0.3$, $\Omega_\Lambda = 0.0$, $\Gamma = 0.21$, $\sigma_8 = 0.86$: *dashed line*), and the best-fit ΛCDM ($\Omega_m = 0.3$, $\Omega_\Lambda = 0.7$, $\Gamma = 0.21$, $\sigma_8 = 0.81$: *dotted line*) models. We fixed $h = 0.7$, which gives a high value for Γ for the SCDM model. Without additional constraints on the cosmological parameters, the lensing results are consistent with a wide range of cosmological models. The error bars are estimated from a large number of random realizations of the data set in which the orientations of the galaxies were randomized. Note that the points at various scales are strongly correlated. Under the assumption that the lensing structures are halfway between the observer and the sources, we have indicated a scale of 1 h_{50}^{-1} Mpc.

cut in apparent magnitude. Bacon et al. (2000) find a variance of $\langle\gamma^2\rangle = (24 \pm 7) \times 10^{-5}$ in $8' \times 8'$ cells. This scale is similar to a radius of $\sim 4'$, for which we find $\langle\gamma^2\rangle = (2.8 \pm 0.5) \times 10^{-5}$. Our signal is much lower than their result. Bacon et al. (2000) note a residual correlation between the shape of the PSF and the galaxies (their Fig. 7), and this might explain their increased variance. We note that because of the large error bar on the measurement of Bacon et al. (2000), the results are consistent at the 3 σ level.

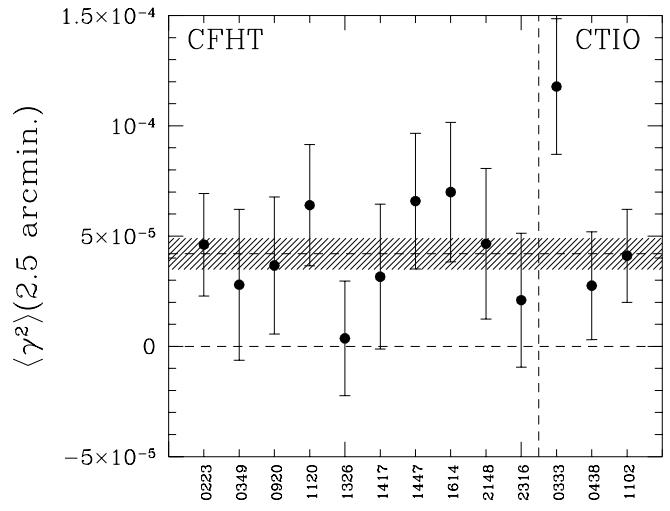

FIG. 9.—Top-hat smoothed variance of the shear for an aperture of radius 2.′5 for the 13 observed patches. The shaded region corresponds to the 1 σ limits around the average. The measurements for the individual patches agree well with the average, indicating that the cosmic variance is small.

5.2. *Constraints on Cosmological Parameters*

As described in § 4, the predicted amplitude of the top-hat smoothed variance depends on the various cosmological parameters and therefore provides a powerful method for constraining these parameters. Unfortunately, several degeneracies exist (e.g., Bernardeau et al. 1997; Jain & Seljak 1997). These studies show that the amplitude of the signal is mainly determined by a combination of σ_8 and Ω_m, although the shape parameter Γ ($\sim\Omega_m h$ in a CDM cosmology) is also important.

As demonstrated by Van Waerbeke et al. (2001), it is possible to partially break the degeneracy between σ_8 and Ω_m if priors on the shape of the power spectrum are assumed. The value of Ω_Λ can be constrained by combining the measurements of the lensing signal for sources at different redshifts, using the fact that the angular diameter distances depend on Ω_Λ. The combination of the weak-lensing measurements and the constraints from studies of the fluctuations of the cosmic microwave background will provide much stronger constraints of the parameters, as the combination will break the degeneracies.

Here we use the measurements of the top-hat smoothed variance to find constraints on Ω_m and σ_8. We assume that the measurements follow a normal distribution. We computed the covariance matrix from a large number of random

realizations of the data, thus including the survey geometry in the noise correlation.

We compute the model predictions using equation (3), under the assumption that $\Gamma = 0.21$ and using the effective redshift distribution discussed in § 4.1. We use this value for Γ to allow for a direct comparison with the results from Van Waerbeke et al. (2001). The predictions are compared with the observations, and the likelihood for the combination of Ω_m and σ_8 is computed. The results for models with $\Omega_\Lambda = 0$ are presented in Figure 11. The contours indicate the 68.3%, 95.4%, and 99.7% confidence limits on the two parameters jointly.

The results for the $\Omega_m + \Omega_\Lambda = 1$ model are presented in Figure 12. The best-fit value for Ω_m is lower than for the OCDM model, but no strong constraints on Ω_m and σ_8 can be placed. Allowing for larger values ($\Gamma \sim 0.7$), the goodness of fit for high-Ω_m models is comparable to that of low-Ω_m models. We note, however, that studies of the galaxy correlation function suggest values for $\Gamma = 0.1$–0.3 (e.g., Dodelson et al. 2001).

The best-fit ΛCDM cosmology yields $\sigma_8 = 0.81^{+0.14}_{-0.19}$ (95% confidence; $\Gamma = 0.21$). For the best-fit OCDM model, we obtain $\sigma_8 = 0.86^{+0.14}_{-0.17}$ (95% confidence). Van Waerbeke et al. (2001) find $\sigma_8 = 0.99^{+0.08}_{-0.10}$ (95% confidence) for an OCDM model, which is in fair agreement with our result, in particular when the uncertainty in the redshift distribution used by Van Waerbeke et al. (2001) is taken into account.

To investigate the agreement between the CFHT and CTIO data, we also compute the best-fit values for σ_8 for the two data sets. We obtain $\sigma_8 = 0.84 \pm 0.09$ (68% confidence) for the CFHT data and $\sigma_8 = 0.76 \pm 0.12$ (68% confidence) for the CTIO data. The values agree well, and the probability of finding a smaller difference is 40%.

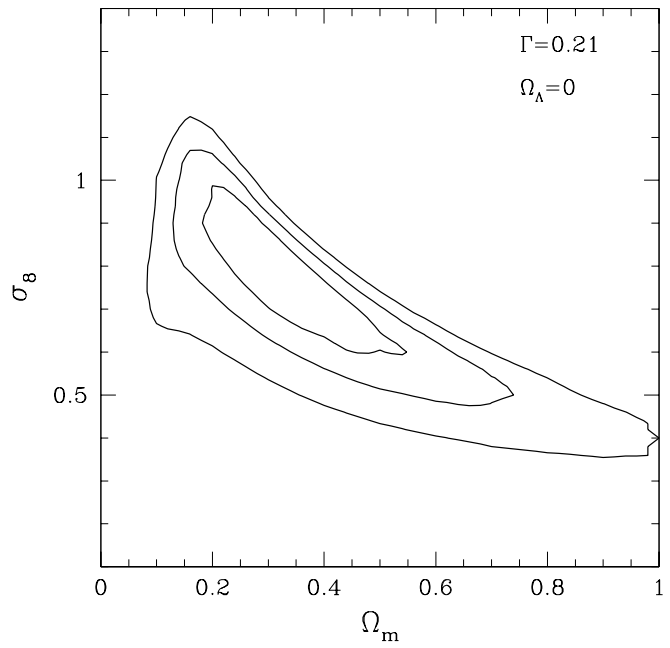

FIG. 11.—Likelihood contours as a function of Ω_m and σ_8, inferred from the analysis of the top-hat smoothed variance. We have used only the measurements at radii $\geq 1'$. The contours have been computed by comparing the measurements with CDM models with $n = 1$, $\Gamma = 0.21$, and $\Omega_\Lambda = 0$. The contours indicate the 68.3%, 95.4%, and 99.7% confidence limits on two parameters jointly.

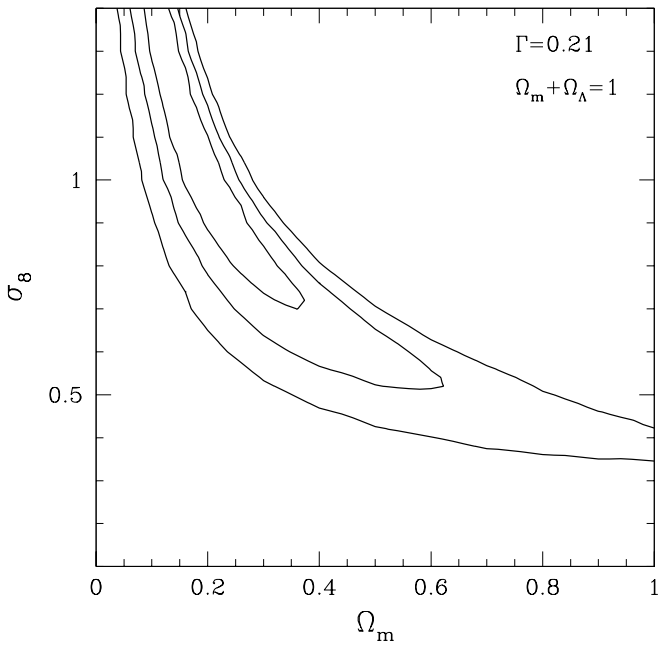

FIG. 12.—Same as Fig. 11, but for an $\Omega_m + \Omega_\Lambda = 1$ CDM cosmology

The RCS probes a different redshift range than the study presented by Van Waerbeke et al. (2001). Although both results are based on the same correction scheme, there are many differences in the various steps in the analyses. Thus, the agreement found here suggests that accurate measurements of cosmic shear can be made.

6. CONCLUSIONS

We have analyzed $\sim$24 deg^2 of R_C-band imaging data from the Red-Sequence Cluster Survey to study the weak-lensing signal caused by intervening large-scale structure. To minimize the effect of cosmic variance, the measurements have been obtained from 13 patches that are widely separated on the sky. We have used data from two different telescopes: $\sim$16.4 deg^2 of CFHT data and $\sim$7.6 deg^2 of CTIO data. We have detected the signal with high confidence on scales ranging from $1'$ to $30'$ using galaxies with $20 < R_C < 24$.

Because of the various observational distortions that need to be corrected for, a careful analysis of the residuals is important. The results suggest that we have successfully corrected for the systematics. In addition, we have compared the measurements from CFHT and CTIO and have found excellent agreement.

Compared to other studies of cosmic shear, the RCS imaging data is relatively shallow. This has the disadvantage that the lensing signal is low. However, the galaxies are larger (which results in smaller corrections for the PSF), and the redshift distribution is known fairly well (which is important for determining cosmological parameters).

Intrinsic alignments of galaxies contaminate the lensing signal. This is particularly important for lensing studies that use low-redshift galaxies. The median redshift of our sample of sources is $\sim$0.5, and predictions of the contribution of the intrinsic alignments suggest it is small for the results presented here. However, the effect of intrinsic alignments is expected to be comparable to the error bars of the full RCS

data set and eventually needs to be corrected for. The RCS will be complemented with *B*- and *V*-band imaging that will provide photometric redshifts for a large number of galaxies. With such a data set, we will be able to measure the intrinsic alignments by selecting galaxies at similar photometric redshifts.

We use the photometric redshift distribution inferred from the Hubble Deep Fields to relate the measured top-hat smoothed variance to estimates of cosmological parameters. Because of degeneracies in the parameters, we can only place constraints on Ω_m and σ_8 jointly. For the currently favored ΛCDM model ($\Omega_m = 0.3$, $\Omega_\Lambda = 0.7$, $\Gamma = 0.21$), we obtain $\sigma_8 = 0.81^{+0.14}_{-0.19}$ (95% confidence), in good agreement with the results from Van Waerbeke et al. (2001).

The RCS data and the observations used by Van Waerbeke et al. (2001) are quite different, and the weak-lensing analyses are also somewhat different. Thus, the agreement found here suggests that accurate measurements of cosmic shear can be made.

It is a pleasure to thank Ludo Van Waerbeke for many discussions and for providing a useful test of the correction scheme used in this paper. We would like to thank the CFHT and CTIO telescope allocation committees for their generous allocation of telescope time. This research is partially supported via an operating grant from NSERC to H. K. C. Y., and M. D. G. acknowledges support from NSERC via PGSA and PGSB scholarships. P. B. H. acknowledges financial support from Chilean grant FONDECYT/1010981. L. F. B.'s research is funded by FONDECYT, Chile under project 1000537.

REFERENCES

Bacon, D., Refregier, A., Clowe, D., & Ellis, R. S. 2001, MNRAS, 325, 1065
Bacon, D., Refregier, A., & Ellis, R. S. 2000, MNRAS, 318, 625
Bartelmann, M., & Schneider, P. 2001, Phys. Rep., 340, 291
Bernardeau, F., Van Waerbeke, L., & Mellier, Y. 1997, A&A, 322, 1
Blandford, R. D., Saust, A. B., Brainerd, T. G., & Villumsen, J. V. 1991, MNRAS, 251, 600
Catelan, P., Kamionkowski, M., & Blandford, R. D. 2001, MNRAS, 320, L7
Chen, H.-W., Fernández-Soto, A., Lanzetta, K. M., Pascarelle, S. M., Puetter, R. C., Yahata, N., & Yahil, A. 1998, preprint (astro-ph/9812339)
Cohen, J. G., Hogg, D. W., Blandford, R. G., Cowie, L. L., Hu, E., Songaila, A., Shopbell, P., & Richberg, K. 2000, ApJ, 538, 29
Crittenden, R. G., Natarajan, P., Pen, U.-L., & Theuns, T. 2001, ApJ, 559, 552
Dodelson, S., et al. 2001, ApJ, submitted (astro-ph/0107421)
Erben, T., Van Waerbeken, L., Bertin, E., Mellier, Y., & Schneider, P. 2001, A&A, 366, 717
Fernández-Soto, A., Lanzetta, K. M., & Yahil, A. 1999, ApJ, 513, 34
Gladders, M. D., & Yee, H. K. C. 2001, in ASP Conf. Ser. 232, The New Era of Wide-Field Astronomy, ed. R. Clowes, A. Adamson, & G. Bromage (San Francisco: ASP), 126
Gladders, M. D., Yee, H. K. C., & Ellingson, E. 2002, AJ, 123, 1
Heavens, A., Refregier, A., & Heymans, C. 2000, MNRAS, 319, 649
Hoekstra, H. 2001, A&A, 370, 743
Hoekstra, H., Franx, M., & Kuijken, K. 2000, ApJ, 532, 88
Hoekstra, H., Franx, M., Kuijken, K., & Squires, G. 1998, ApJ, 504, 636
Hoekstra, H., Yee, H. K. C., & Gladders, M. D. 2001a, ApJ, 558, L11
Hoekstra, H., et al. 2001b, ApJ, 548, L5
Hu, W. 1999, ApJ, 522, L21
Hu, W., & Tegmark, M. 1999, ApJ, 514, L65
Jain, B., & Seljak, U. 1997, ApJ, 484, 560
Kaiser, N. 1992, ApJ, 388, 272
Kaiser, N., Squires, G., & Broadhurst, T. 1995, ApJ, 449, 460
Kaiser, N., Wilson, G., & Luppino, G. A. 2000, ApJ, submitted (astro-ph/0003338)
Kuijken, K. 1999, A&A, 352, 355
Luppino, G. A., & Kaiser, N. 1997, ApJ, 475, 20
Mackey, J., White, M., & Kamionkowski, M. 2002, MNRAS, in press (astro-ph/0106364)
Maoli, R., Van Waerbeke, L., Mellier, Y., Schneider, P. Jain, B., Bernardeau, F., Erben, T., & Fort, B. 2001, A&A, 368, 766
Mellier, Y. 1999, ARA&A, 37, 127
Peacock, J. A., & Dodds, S. J. 1996, MNRAS, 280, L19
Refregier, A. 2001, MNRAS, submitted (astro-ph/0105178)
Schneider, P. 1998, ApJ, 498, 43
Schneider, P., Van Waerbeke, L., Jain, B., & Kruse, G. 1998, MNRAS, 296, 873
Tyson, J. A., Wenk, R. A., & Valdes, F. 1990, ApJ, 349, L1
Van Waerbeke, L., et al. 2000, A&A, 358, 30
———. 2001, A&A, 374, 757
Wittman, D. M., Tyson, J. A., Kirkman, D., Dell'Antonio, I., & Bernstein, G. 2000, Nature, 405, 143